In-plane magnetic anisotropies in Fe_3O_4 films on vicinal MgO(100)

L. McGuigan* and R. C. Barklie
School of Physics, Trinity College, Dublin 2, Ireland

R. G. S. Sofin, S. K. Arora, and I. V. Shvets
CRANN, School of Physics, Trinity College, Dublin 2, Ireland

(Received 4 January 2008; revised manuscript received 29 February 2008; published 21 May 2008)

Ferromagnetic resonance was used to study the influence of vicinal (miscut) angle and film thickness on in-plane fourfold and uniaxial magnetic anisotropies in epitaxial Fe_3O_4 films grown on vicinal MgO(100) surfaces. The in-plane fourfold anisotropy constant $K_{4\|}$ is approximately the same for all films but the dominant in-plane uniaxial constant $K_{2\|}$ varies linearly with the inverse Fe_3O_4 layer thickness and approximately quadratically with the vicinal angle. A second, weaker, in-plane uniaxial term is evident for the film on a larger miscut (10°) substrate. The easy axis of the dominant in-plane uniaxial term is perpendicular to the step edges. The dominant in-plane uniaxial anisotropy has one term inversely proportional to the film thickness that is associated with anisotropy localized at the interface and a second term that is independent of film thickness; the latter may arise from the preferential alignment of antiphase boundaries with the step edges.

DOI: 10.1103/PhysRevB.77.174424 PACS number(s): 75.70.Ak, 75.30.Gw, 76.50.+g

I. INTRODUCTION

The magnetic properties of ferromagnetic thin films grown epitaxially on a vicinal substrate surface are of interest because of both their technological and scientific importance.[1–3] There have been several studies of such films on these step arrays: Fe/stepped Ag(100),[4–6] Fe/stepped Au(100),[6] Fe/stepped W(001),[7,8] Fe/stepped W(110),[9] Fe/stepped Mo(110),[10] $Fe_{1-x}Co_x$/stepped GaAs(100),[11] Co/stepped Cu(100),[12,13] and $CoPt_3$/stepped MgO(100).[14] They all show that the parallel step arrays induce an in-plane uniaxial magnetic anisotropy. However, the easy axis of magnetization associated with this anisotropy is sometimes parallel to the step edges[3,5,10,12,13] and at other times perpendicular to them.[6–8,14] As noted above, measurements have so far been mostly confined to films of Fe or Co and there are no reports or similar investigations for half metallic ferromagnetic materials. Half metallic ferromagnetic (HMFM) materials with their 100% spin polarization are expected to have an important role in spin electronic devices. Examples of such HMFM materials are rare earth doped manganites, double perovskites, CrO_2, and magnetite (Fe_3O_4). Fe_3O_4 with its high Curie temperature of 858 K (Ref. 15) is particularly attractive. Epitaxial films of Fe_3O_4 are often grown on (100) MgO because there is only a small lattice mismatch of 0.34%. However, because the Fe_3O_4 unit cell is almost twice the size of the MgO unit cell and because films form by the coalescence of separately nucleated islands, such films contain antiphase boundaries (APBs).[16–18] Across these boundaries, the oxygen lattice remains unaffected but the cation lattice is displaced and this alters the magnetic exchange interactions at the boundary. As shown by Margulies *et al.*,[16] intrasublattice exchange interactions dominate across the boundaries that thus separate oppositely magnetized regions. It was also shown[16] that this accounts for the difficulty in saturating the magnetization of magnetite films even with magnetic fields up to several tesla. Also affected by the presence of APBs is the magnetoresistance (MR) behavior of the films.[19,20] To selectively extract the contribution of APBs to the MR, Arora *et al.*[20] measured the MR in directions $[0\bar{1}1]$ and [011], parallel and perpendicular to the step edges formed by the epitaxial growth of Fe_3O_4 films on vicinal (100) MgO substrates with miscut angles of 0.5° and 2°. They showed that the APBs would preferentially align parallel to the step edges and so were able to show that the observed anisotropy in MR could be attributed to the presence of the APBs. A schematic diagram of a structure with an APB along the step edge is shown in Fig. 1. More detailed discussion of the formation of APBs along step edges is given elsewhere.[20]

In this paper, we present the results of a systematic study of the in-plane magnetic anisotropy of Fe_3O_4 films grown epitaxially on vicinal (100) MgO substrates. Since ferromagnetic resonance (FMR) is particularly sensitive to changes in

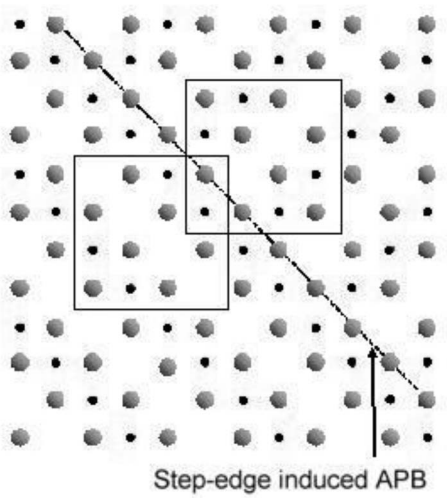

FIG. 1. Schematic diagram showing one possibility of formation of a step induced APB. The large and small circles represent O^{2-} and *B*-site Fe^{3+}/Fe^{2+} ions, respectively. The boxes indicate the magnetite unit cell and show the change in structure as the APB is crossed.

such anisotropy,[21] this is the technique we have used. We have examined the effect of changing both the vicinal angle in the range 2°–10° for a fixed film thickness of 45 nm and of changing the film thickness from 30 to 70 nm at a fixed vicinal angle of 2°. Measurements of both the resonance field (H_R) and the linewidth ($\Delta H_{\mathrm{p.p.}}$) were made as a function of the direction of the magnetic field within the plane of the films and from these we extract the anisotropy fields and their dependence on both vicinal angle and film thickness.

II. EXPERIMENTAL PROCEDURE

A. Sample preparation

Two sets of Fe_3O_4 films were grown by molecular beam epitaxy (MBE) on single crystal MgO substrates vicinal to (100). All the substrates were miscut along the [011] direction so that the edges of the terraces are in the $[0\bar{1}1]$ direction. Three different substrates were used with a miscut angle, α, of 2°, 5°, or 10°. Films of thickness, d, of 45 nm were grown on each of these substrates and, in addition, films of thicknesses 30 and 70 nm were deposited on the 2° miscut substrates. The substrates were cleaned chemically prior to insertion into the growth chamber and were further cleaned *in situ* at 600 °C in UHV for 1 h followed by annealing in oxygen at 1×10^{-5} torr for 6 h. The Fe_3O_4 films were grown by the electron beam evaporation of metallic iron (99.999%) in the presence of free oxygen radicals generated by an electron cyclotron resonance plasma source. The substrate temperature during growth was 250 °C. Further details of the growth procedure are given elsewhere.[20] Reflection high energy electron diffraction (RHEED) measurements confirm that the films grew in a layer-by-layer mode at a rate of 0.3 Å/s. As reported previously,[20] RHEED images of the 2° MgO substrate taken after the UHV heat treatment, but before film deposition, give a miscut angle of 2.1°. Further RHEED measurements of this substrate after deposition of the 45 nm Fe_3O_4 film showed[20] that the average terrace width is 5.7 ± 0.5 nm, consistent with the miscut angle. High resolution x-ray diffraction (HRXRD) rocking curves showed[20] that, for the above film, the out-of-plane lattice constant is 0.8372 nm whereas the in-plane lattice constant is 0.8423 nm, twice that of the MgO substrate (0.4213 nm). This gives the volume of the unit cell as 0.594 nm^3, in full agreement with that of stoichiometric magnetite. It was inferred[20] from the *in situ* RHEED and the *ex situ* HRXRD measurements that the films grow pseudomorphically and maintain one-to-one registry with the MgO substrate.

B. Ferromagnetic resonance measurements

FMR measurements were made at room temperature using a rectangular TE_{102} mode cavity operating at about 9.6 GHz. Samples were mounted horizontally at the end of a vertical, spin-free, quartz rod that could be rotated by a goniometer such that the magnetic field direction varied within the film plane. 100 kHz field modulation was used and so the FMR signal corresponds to the field derivative of the absorbed microwave power. The resonance field was taken as the field value at which the signal crosses the base line between the derivative extrema and was determined typically to an accuracy of 5 Oe. The absolute orientation was determined to within about 5° but changes in orientation could be measured to within 0.1°. The magnetic field position was calibrated using an NMR magnetometer and an electron paramagnetic resonance reference signal due to F^+ centers in MgO with a known g value.

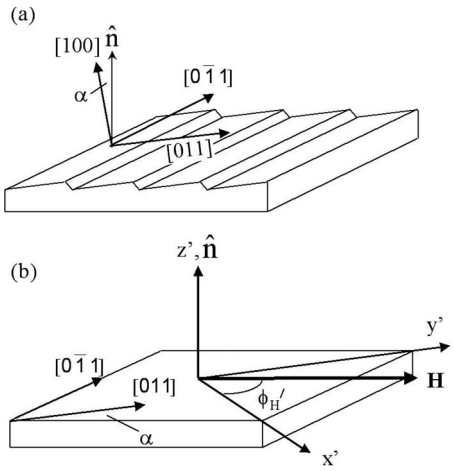

FIG. 2. Schematic diagram of (a) the vicinal MgO (100) substrate characterized by (011) terraces with steps parallel to $[0\bar{1}1]$ and (b) the film. $\hat{n}$ is the normal to the film and x' and y' are the projections of [010] and [001], respectively, within the film plane. $\boldsymbol{H}$ lies in the film plane.

Figure 2(a) shows a schematic diagram of a vicinal MgO (100) substrate. The overall surface of the film is parallel to a plane formed by rotating the (100) plane by α degrees about the $[0\bar{1}1]$ direction where $[0\bar{1}1]$ is the mean direction of the atomic step edges. The direction of $\boldsymbol{H}$ within the film plane is given by the angle ϕ'_H, as shown in Fig. 2. For all films the angle ϕ'_H differs by less than 1° from ϕ_H, the angle between [010] and the projection of $\boldsymbol{H}$ in the (100) plane.

III. EXPERIMENTAL RESULTS

A. In-plane angular dependence of resonance field

A single FMR line was observed for all the samples. For each sample, we measured the dependence of the ferromagnetic resonance field, H_R, on the direction of the external magnetic field, $\boldsymbol{H}$, as it was rotated within the plane of the film. Figure 3 shows this in-plane angular dependence for the Fe_3O_4 films of different thicknesses (30–70 nm) on MgO (100) substrates with a fixed vicinal angle of 2°.

Figure 3(a) shows that the 70 nm film displays the fourfold anisotropy to be expected for a cubic crystal. The minima in H_R occur at $\phi'_H=45°, 135°, \ldots$ corresponding to the projections within the film plane of the [011]-type directions; this is consistent with previous FMR measurements[22,23] of thin Fe_3O_4 films on (100) MgO that also find the minima to be in [011]-type directions. Details of the analysis are given in the next section and we just note here that, as shown in Fig. 3(a), the angular dependence of

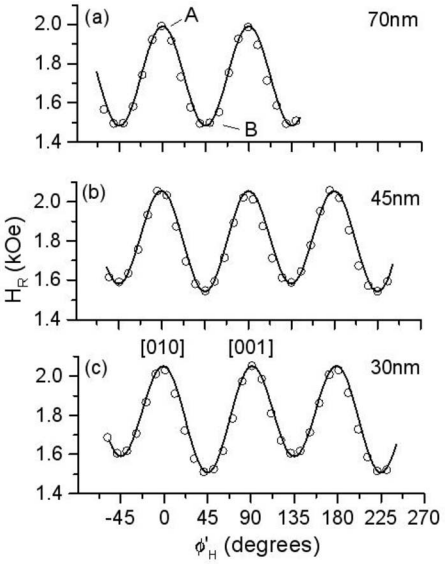

FIG. 3. The in-plane ferromagnetic resonance field, H_R, as a function of angle ϕ'_H for Fe_3O_4 on 2° miscut vicinal MgO(100) with film thicknesses (a) 70, (b) 45, and (c) 30 nm. The solid lines are fits using Eq. (4) with parameters given in Table I. Note that the curvatures at points *A* and *B* are very similar.

H_R fits well to that expected for cubic magnetocrystalline anisotropy. However, Figs. 3(b) and 3(c) show that for the 45 and 30 nm films, the value of the resonance field for $\boldsymbol{H}$ parallel to [011], or, to be more exact, to its projection in the film plane, clearly differs from that for $\boldsymbol{H}$ parallel to $[0\bar{1}1]$. This implies an inequivalence of the [011] and $[0\bar{1}1]$ directions that is a manifestation of an in-plane uniaxial anisotropy superimposed on the cubic anisotropy; the former increases in strength with decreasing thickness as shown in Fig. 3. As discussed in detail in Sec. IV and as shown in Figs. 3(b) and 3(c), a good fit to the angular dependence is obtained by including an in-plane uniaxial anisotropy term with axis along the step edge direction $[0\bar{1}1]$; however, it is clear that the uniaxial easy axis is in the [011] direction, perpendicular to the step edge.

Figure 4 shows the effect on the in-plane angular dependence of H_R of changing the vicinal angle, α, from 2° to 10° at a fixed film thickness of 45 nm. Figure 4(b) shows that increasing α from 2° to 5° leads to an increase in the magnitude of the uniaxial term that manifests itself as an increase in the difference in the H_R value for the [011] and $[0\bar{1}1]$ directions. Once again, the combination of the cubic term with a single in-plane uniaxial term yields a good fit as shown in Fig. 4(b). Figure 4(c) shows the angular dependence of H_R at $\alpha=10°$. Two points are worth noting about this plot. Firstly, H_R is further decreased along [011] and increased along $[0\bar{1}1]$ (to such an extent in the latter direction that the dip has disappeared) and this indicates a further increase in the magnitude of the previous uniaxial term. Secondly, there is an inequivalence in the directions [001] and [010]; we find that this can be accounted for by the inclusion of a second but weaker in-plane uniaxial term, this time with axis along [010], and Fig. 4(c) shows that with this a good fit can be obtained.

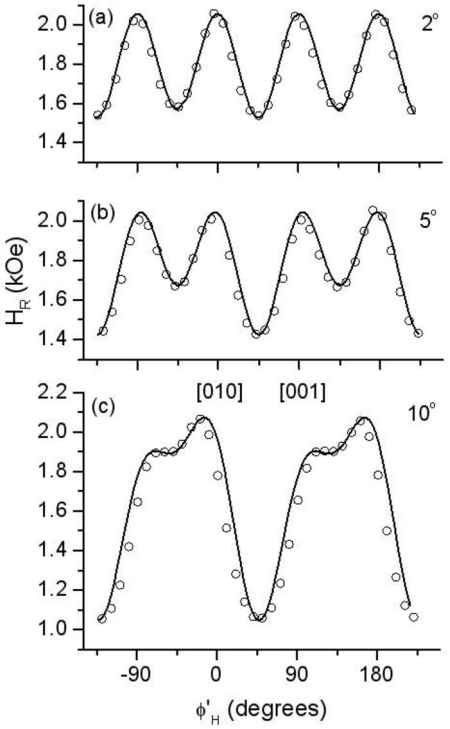

FIG. 4. The in-plane ferromagnetic resonance field, H_R, as a function of angle ϕ'_H for 45 nm Fe_3O_4 on vicinal MgO(100) with miscut angles of (a) 2°, (b) 5°, and (c) 10°. The solid lines are fits using Eq. (4) with parameters given in Table I.

B. In-plane angular dependence of linewidth

The dependence of the peak-to-peak FMR linewidth, $\Delta H_{\text{p.p.}}$, on the applied field direction within the film plane was measured for all samples. Figure 5 shows the in-plane angular dependence of $\Delta H_{\text{p.p.}}$ for the films with thicknesses 70, 45, and 30 nm on the $\alpha=2°$ substrate; also shown to aid comparison is a plot of H_R versus angle ϕ'_H for the film with $\alpha=2°$, $d=45$ nm. It is clear that changing the thickness in this range has a little effect on the linewidth. For the 70 nm film $\Delta H_{\text{p.p.}}$ varies approximately in step with H_R with minima when $\boldsymbol{H}$ is parallel to the in-plane easy axes in the [011]-type directions; there also appear to be weaker minima along the [010]-type directions. For the other two films, there also appear to be linewidth minima along the [011]- and [010]-type directions. The linewidth variation is quite small, ranging from about 180 to 200 Oe for the 70 and 45 nm films, and from 190 to 225 Oe for the 30 nm film.

In contrast to the small effect of changing the film thickness, Fig. 6 shows that changing the angle α at a fixed thickness, d, of 45 nm, has a much larger effect on the linewidth. To aid comparison, the angular dependence of H_R for $\alpha=5°$, thickness $d=45$ nm is also shown in Fig. 6(d). It is clear that for $\alpha=5°$ and 10°, the minima of $\Delta H_{\text{p.p.}}$ are again along the [011]-type directions but now the linewidth minimum along $[0\bar{1}1]$ is clearly less than that along [011]. The inequivalence of the [011] and $[0\bar{1}1]$ directions is therefore also revealed in the linewidth. Surprisingly, as Fig. 6 shows, the $\Delta H_{\text{p.p.}}$ angular dependence pattern is shifted in angle by

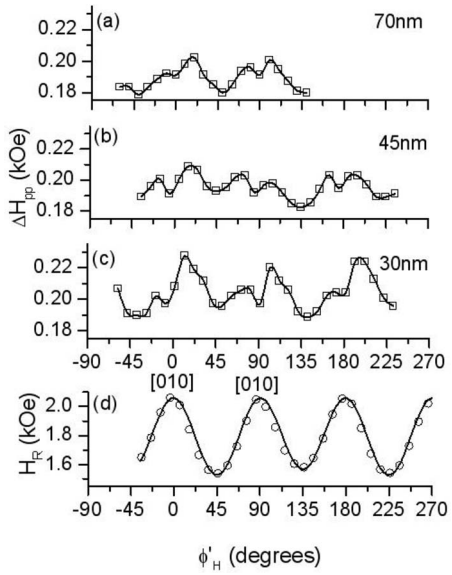

FIG. 5. The in-plane ferromagnetic resonance linewidth, $\Delta H_{\text{p.p.}}$, as a function of angle ϕ'_H for films with $\alpha=2°$ and thicknesses, d, of (a) 70, (b) 45, and (c) 30 nm; the lines are guides to the eyes. (d) H_R versus angle ϕ'_H for the film with $\alpha=2°$, $d=45$ nm with theoretical fit.

90° relative to that of H_R. Finally, we note that increasing α from 5° to 10° amplifies the variation in linewidth and also increases the mean value of $\Delta H_{\text{p.p.}}$.

IV. ANALYSIS

A. Angular dependence of the resonance field

We begin by considering what is the appropriate expression for the magnetic free energy density of the Fe_3O_4 films grown on the vicinal (100) MgO substrates. The measurements of the lattice parameters, given in Sec. II, show that there is a slight tetragonal distortion for the film with $\alpha=2°$, $d=45$ nm. From our earlier studies,[24] we know that the same is true for the other samples in the thickness range used in the study. The step edges reduce the in-plane symmetry from fourfold to twofold. Therefore, the formula for the free energy density, F, for a cubic crystal does not apply. We use the formula for a crystal with both in-plane and out-of-plane fourfold and twofold anisotropies given by Liu and Furdyna[25] as follows:

$$F = -\tfrac{1}{2}M\{2H[\cos\theta\cos\theta_H + \sin\theta\sin\theta_H\cos(\phi-\phi_H)] - 4\pi M\cos^2\theta + H_{2\perp}\cos^2\theta + \tfrac{1}{2}H_{4\perp}\cos^4\theta + H_{2\parallel}\sin^2\theta\sin^2(\phi-\pi/4) + \tfrac{1}{2}H_{4\parallel}\tfrac{1}{4}(3+\cos 4\phi)\sin^4\theta\}. \quad (1)$$

Although the sources of the anisotropy in our case are not exactly the same as those observed by Liu and Furdyna,[25] this formula is phenomenologically correct.

For a (100) film, θ and θ_H are the angles between [100] and the magnetization $\boldsymbol{M}$ and applied field $\boldsymbol{H}$, respectively. ϕ and ϕ_H are the angles between [010] and the projections of $\boldsymbol{M}$ and $\boldsymbol{H}$, respectively, in the (100) plane. The first term is the Zeeman energy $-\boldsymbol{M}\cdot\boldsymbol{H}$ and the second, $2\pi M^2\cos^2\theta$ is the demagnetizing energy (or so-called shape anisotropy) for an infinite plane, to which the film is an approximation. The other terms that are most relevant here come from the magnetic anisotropy. The anisotropy fields H_i in Eq. (1) are defined in terms of anisotropy energies K_i as $H_i=2K_i/M$. The in-(100)-plane, $K_{4\parallel}$, and perpendicular to (100) plane, $K_{4\perp}$, fourth order terms arise from the cubic anisotropy and differ because of the tetragonal distortion. The second order uniaxial anisotropy term $K_{2\perp}$, with axis along [100], comes from the vertical lattice distortion and from the broken symmetry of the crystal field acting on the (100) interface atomic layer, as pointed out elsewhere.[21,25] $K_{2\perp}$ may depend on film thickness. In the present case, perhaps, the most important term is the in-(100)-plane uniaxial anisotropy energy density $K_{2\parallel}$ that implies a difference in energy between the cases of $\boldsymbol{H}\parallel[011]$ and $\boldsymbol{H}\parallel[0\bar{1}1]$. This is to be expected since the step edges are parallel to $[0\bar{1}1]$. It is to be expected that $K_{2\parallel}$ depends on both vicinal angle and film thickness.

The resonance frequency ω is given by[26,27]

$$\left(\frac{\omega}{\gamma}\right)^2 = \frac{1}{M^2\sin^2\theta}\left[\frac{\partial^2 F}{\partial\phi^2}\frac{\partial^2 F}{\partial\theta^2} - \left(\frac{\partial^2 F}{\partial\phi\partial\theta}\right)^2\right], \quad (2)$$

where γ is the gyromagnetic ratio.

Equations (1) and (2) yield the general resonance condition[25]

$$\left(\frac{\omega}{\gamma}\right)^2 = [(H_R\times a_1+b_1)(H_R\times a_1+b_2)-b_3^2], \quad (3)$$

where

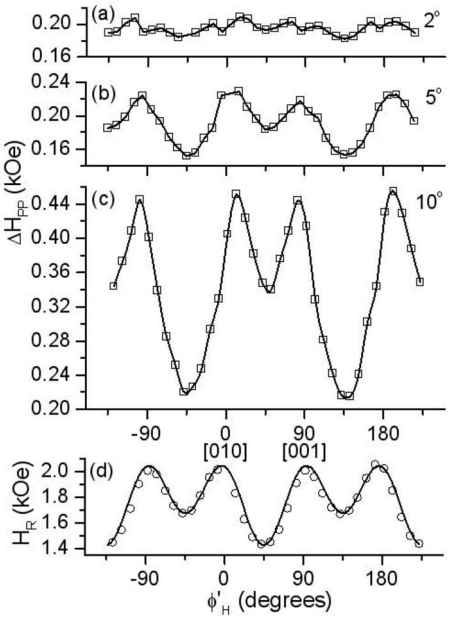

FIG. 6. The in-plane ferromagnetic resonance linewidth, $\Delta H_{\text{p.p.}}$, as a function of angle ϕ'_H for Fe_3O_4 films with $d=45$ nm and vicinal angles, α, of (a) 2°, (b) 5°, and (c) 10°; the lines are guides to the eyes. (d) H_R versus ϕ'_H for the film with $d=45$ nm, $\alpha=5°$ with theoretical fit.

TABLE I. Parameters extracted from fits of theoretical model to the experimental data for Fe_3O_4 films of thickness, d, on vicinal MgO(100) substrates miscut by angles α.

α (°)	d (nm)	$H_{2\parallel}$ (Oe)	$H_{4\parallel}$ (Oe)	$4\pi M_{\text{eff}}$ (kOe)	$H'_{2\parallel}$ (Oe)
2	70	-0 ± 5	-305 ± 7	4.52 ± 0.03	
2	45	-23 ± 5	-305 ± 7	4.23 ± 0.03	
2	30	-47 ± 5	-307 ± 7	4.28 ± 0.03	
5	45	-142 ± 5	-295 ± 7	4.34 ± 0.03	
10	45	-480 ± 20	-230 ± 20	5.2 ± 0.2	190 ± 20

$$a_1=\cos\theta\cos\theta_H+\sin\theta\sin\theta_H\cos(\phi-\phi_H),$$

$$b_1=-\left[4\pi M-H_{2\perp}+H_{2\parallel}\cos^2\left(\phi+\frac{\pi}{4}\right)\right]\times\cos 2\theta+H_{4\perp}\frac{\cos2\,\theta+\cos4\,\theta}{2}+H_{4\parallel}\left(\frac{\cos4\,\theta-\cos2\,\theta}{2}\right)\frac{3+\cos4\,\phi}{4},$$

$$b_2=-(4\pi M-H_{2\perp})\cos^2\theta+H_{4\parallel}\sin^2\theta\times\left(\cos4\,\phi-\cos^2\theta\frac{3+\cos4\,\phi}{4}\right)+H_{4\perp}\cos^4\theta-H_{2\parallel}\left\{\sin2\,\phi+\left[\cos\theta\cos\left(\phi+\frac{\pi}{4}\right)\right]^2\right\},$$

$$b_3=\tfrac{1}{2}\cos\theta\left(\tfrac{3}{2}H_{4\parallel}\sin4\,\phi\sin^2\theta+H_{2\parallel}\cos2\,\phi\right).$$

We now consider what is the appropriate resonance condition for the present case, where the applied field $\boldsymbol{H}$ lies within the film plane, which is tilted from the (100) plane by an angle α about the step edge direction $[0\bar{1}1]$. We define a new set of axes x', y', and z' as shown in Fig. 2, where z' is the film normal and x' and y' are the projections of [010] and [001], respectively, into the film plane. Since in our experiments $\boldsymbol{H}$ lies in the film plane, we have taken ϕ'_H as the angle between $\boldsymbol{H}$ and the x' direction. Similarly, since $\boldsymbol{M}$ will also lie within or very close to the film plane, we take ϕ' as the angle between $\boldsymbol{M}$ and x'. The angle θ'_H between $\boldsymbol{H}$ and z' (the film normal) is 90° and also $\theta'\approx90°$. We estimate that, for all $\alpha\leqslant10°$, $|\phi_H-\phi'_H|<1°$ and so to very good approximation we take $\phi_H=\phi'_H$. It is also reasonable to suppose that $\phi=\phi'$. As regards the other angles, θ_H varies between 90° for $\boldsymbol{H}\|[0\bar{1}1]$ (at $\phi'_H=-45°$) and $90°+\alpha$ for $\boldsymbol{H}\|[011]$ (at $\phi'_H=45°$); a very similar variation for θ is expected. If we make the reasonable approximation that in our case, $\theta\approx\theta_H$ and $\theta'\approx\theta'_H$, then the errors in taking $\theta_H\approx\theta'_H$ amount to only about 3%, 6%, and 3% in the cases of $\sin^2\theta$, $\sin^4\theta$, and $\cos^2\theta$, respectively. Since these errors are small, we make the simplifying assumption that $\theta=\theta'=\theta_H=\theta'_H=90°$, as well as $\phi=\phi'$ and $\phi_H=\phi'_H$ to obtain the resonance condition for our case to be

$$\left(\frac{\omega}{\gamma}\right)^2=\left[H\cos(\phi-\phi_H)-H_{2\parallel}\cos\left(2\phi-\frac{\pi}{2}\right)+H_{4\parallel}\cos4\,\phi\right]\times\left[H\cos(\phi-\phi_H)+4\pi M_{\text{eff}}+H_{2\parallel}\sin^2\left(\phi-\frac{\pi}{4}\right)+H_{4\parallel}\frac{1}{4}(3+\cos4\,\phi)\right],\tag{4}$$

where $4\pi M_{\text{eff}}=4\pi M-H_{2\perp}$. It is worth noting that, because in our experiments $\boldsymbol{H}$ lies in the film plane, the demagnetization contribution to the energy density should be zero.

When the magnetization lags appreciably behind the in-plane applied field, a plot of resonance field versus ϕ_H exhibits a smaller curvature for $\boldsymbol{H}$ along the easy axis than for $\boldsymbol{H}$ along the hard axis[28,29] but, as shown in Fig. 3(a), the curvatures at points A and B are very similar and therefore we also take $\phi'=\phi'_H$.

Figures 3(a)–3(c), 4(a), and 4(b) show that the data fits well to the angular dependence predicted by Eq. (4) with $\phi'=\phi'_H$. The values of $H_{2\parallel}$, $H_{4\parallel}$, and $4\pi M_{\text{eff}}$ used in the fits are given in Table I. The fits were evaluated with $g=2.12$.[30] Figure 4(c) shows that at $\alpha=10°$, in addition to the inequivalence of $\boldsymbol{H}\|[011]$ and $\boldsymbol{H}\|[0\bar{1}1]$, there is an inequivalence of $\boldsymbol{H}\|[010]$ and $\boldsymbol{H}\|[001]$ that is not accounted for by Eq. (4). One possible reason for this inequivalence could be the presence of kinks in the step edge. It is possible that for the larger values of α, miscutting the MgO (100) surface along the [011] direction may not produce exactly straight step edges, but rather a ragged edge, with some portions along $[0\bar{1}1]$ and others along another direction. Since imaging of the MgO surface is difficult in ambient due to the formation of hydroxide, we cannot confirm that this is the case; however, the

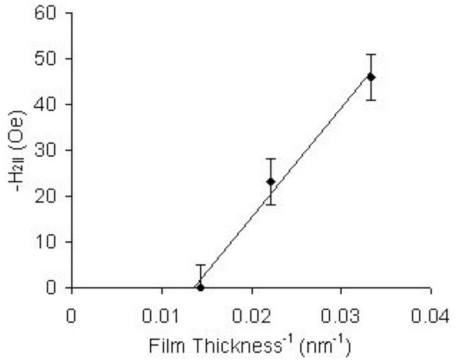

FIG. 7. Dependence of the uniaxial anisotropy field $H_{2\|}$ on 1/film thickness; the line is a best fit with parameters given in the text. $\alpha=2°$.

presence of step portions along one of the principal crystal axis directions could induce this additional inequivalence that is observed. In an attempt to account for this, we introduce a further in-plane uniaxial anisotropy density term F'_A with axis along [010] so that

$$F'_A = -K'_{2\|}\beta_x^2 = -K'_{2\|}\sin^2\theta\sin^2\phi,$$

where β_x is the direction cosine between $\boldsymbol{H}$ and the [010] direction.

With the same assumptions as before, this leads to the resonance condition

$$\left(\frac{\omega}{\gamma}\right)^2 = \left[H\cos(\phi-\phi_H) - H_{2\|}\cos\left(2\phi-\frac{\pi}{2}\right) + H_{4\|}\cos 4\phi - H'_{2\|}\cos 2\phi\right] \times\left[H\cos(\phi-\phi_H) + 4\pi M_{\text{eff}} + H_{2\|}\sin^2\left(\phi-\frac{\pi}{4}\right) + H_{4\|}\frac{1}{4}(3+\cos 4\phi) + H'_{2\|}\sin^2\phi\right]. \quad (5)$$

Figure 4(c) shows that Eq. (5) gives a good fit to the data. The parameters used in the fit are given in Table I.

Table I shows that both $H_{2\|}$ and $H_{4\|}$ are negative and that the one value of $H'_{2\|}$ is positive. This implies that, as regards anisotropy contributions to the free energy density, the cubic term gives a minimum along [011]-type directions, the first uniaxial term gives a minimum along [011], which is perpendicular to the step edge direction $[0\bar{1}1]$, and the second uniaxial term gives a minimum along [001].

The most interesting parameter for these films is the uniaxial anisotropy field $H_{2\|}$ $(=2K_{2\|}/M)$. Table I shows that the magnitude of $H_{2\|}$ increases as the film thickness, d, decreases and, although we only have three d values, Fig. 7 suggests that, for $\alpha=2°$, the dependence of $H_{2\|}$ on d is given by

$$H_{2\|} = A + \frac{B}{d}, \quad (6)$$

with $A=33\pm6$ Oe and $B=-(2.4\pm0.2)\times10^{-4}$ Oe cm. In addition, Fig. 8(a) shows that, for a film thickness of 45 nm, $H_{2\|}$ varies almost quadratically with α the log-log plot of Fig. 8(b) gives the exponent to be 1.89 ± 0.06. An expression for $H_{2\|}$ that is consistent with these results is

$$H_{2\|} = \left(\frac{90}{\pi}\right)^2\left(A+\frac{B}{d}\right)\alpha^2, \quad (7)$$

where $H_{2\|}$ is in Oe, α in rad, and A and B have the values given above. Equation (7) gives the values of $H_{2\|}$ in Oe of −1.3, −20.3, −47, −127, and −507 for (α,d) of (2°, 70 nm), (2°, 45 nm), (2°, 30 nm), (5°, 45 nm), and (10°, 45 nm) that agree well with the measured values of 0 ± 5, -23 ± 5, -47 ± 5, -142 ± 5, and -480 ± 20, respectively.

We now consider what may give rise to this expression for $H_{2\|}$ and begin with the term in α^2/d. Kawakami *et al.*[5] showed that for a stepped (001) bcc film, there should be an

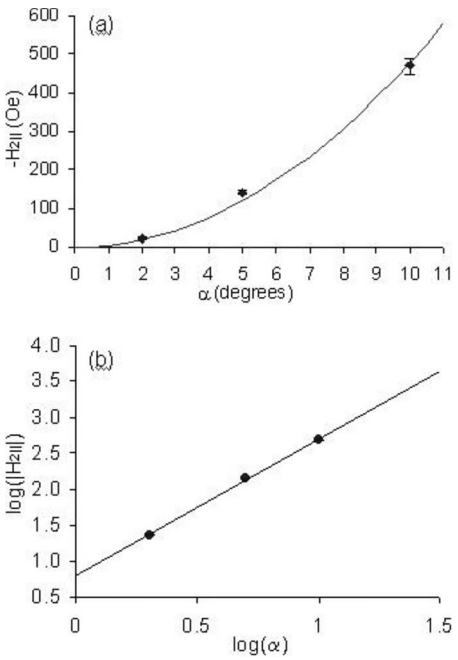

FIG. 8. Dependence of $H_{2\|}$ on vicinal angle α shown with (a) linear scales and (b) log scales. Shown are fits in (a) of $-H_{2\|}=4.8\alpha^2$ and in (b) of $\log(|H_{2\|}|)=1.89\log\alpha+0.80$. Each film has a thickness of 45 nm.

in-plane uniaxial anisotropy $(K_{sp}/a-K_s)\alpha^2/d$ where K_s and K_{sp} are the surface and step anisotropy constants, respectively, and a is the step height. This result was obtained using a model based on that proposed by Neel,[31] which kept only its functional form reflecting the symmetry of the lattice. The in-plane uniaxial anisotropy of bcc Fe grown on stepped Ag(001) (Ref. 5) and of Fe on curved W(001) (Ref. 8) is found to show an α^2 dependence, similar to the one in magnetite. By contrast, for an fcc lattice, the steps can give rise to a linear dependence of the induced anisotropy on step density as has been observed[12] for fcc Co on curved Cu (001). Spinel Fe_3O_4 is a lot more complex than a metal, for example Fe, and first-principles derivation of anisotropy cannot readily be done. However, in order to get an estimate of the anisotropy constants, we assume that our α^2/d term in Eq. (7) can be identified with that for the bcc film so that

$$\left(\frac{90}{\pi}\right)^2\frac{B\alpha^2}{d} \equiv 2\left(\frac{K_{sp}}{a}-K_s\right)\frac{\alpha^2}{dM}, \tag{8}$$

with $B=-(2.4\pm0.2)\times10^{-4}$ Oe cm. For the $\alpha=2°$ films, the mean terrace width is 5.7 nm,[20] and so the step height $a \approx 0.2$ nm; we assume the same value of a for all films. From previous measurements of $M(H)$,[20] we find that $M \approx 432$ emu/cm^3 in the field range of our FMR experiments. Therefore, we obtain $(K_{sp}/a-K_s)\approx-42$ erg/cm^2. If $K_{sp}/a \gg K_s$, then $K_{sp}\approx-8.5\times10^{-7}$ erg/cm, a value greater than that of 5.73×10^{-8} erg/cm found for Fe/stepped Ag(001).[5]

Now, we turn our attention to the other term in Eq. (7), $(90/\pi)^2A\alpha^2$, which is independent of film thickness. Its independence of film thickness implies that it can be associated with a uniaxial volume contribution K_U^V, so that we may write

$$H_{2\|} = \left(\frac{90}{\pi}\right)^2\left(A+\frac{B}{d}\right)\alpha^2 \equiv 2\left(K_U^V+\frac{1}{d}\left[\frac{K_{sp}}{a}-K_s\right]\right)\frac{\alpha^2}{M}. \tag{9}$$

Using the previous values of A and M, we obtain $K_U^V \approx 6\times10^6$ erg/cm^3. Leeb *et al.*[6] found that the in-plane uniaxial anisotropy constants, K_u^{eff}, for Fe films on vicinal Ag(001) and Au(001) fit to a similar expression

$$K_U^{eff} = K_U^V + \frac{2K_U^S}{d}$$

although the values of $K_U^V=-2.3\times10^4$ erg/cm^3 and -1.6×10^4 erg/cm^3 found for Fe/Ag and Fe/Au, respectively, are much smaller than the value we find for Fe_3O_4/MgO. It is interesting to note that for Fe/curved W(001) and Fe/vicinal Ag(001),[4] the in-plane uniaxial anisotropy was found to be thickness independent although varying as α^2. In these latter cases, the thickness independence was attributed to the presence of strain. Wu *et al.*[4] suggested that $1/d$ dependence was seen by Leeb *et al.*[6] because the strain was relaxed, possibly as a result of depositing the Ag and Au seed layers on a stepped GaAs (001) substrate with vicinal angle of 2°. HRXRD studies of our films show that strain is isotropic within the plane of the film[19] and cannot contribute to the uniaxial volume term K_U^V. Instead of being linked to strain, the K_U^V term may be related to the preferential alignment of the APBs parallel to the step edges.[20] These defects propagate though the entire thickness of the film could produce an anisotropy energy proportional to the film's volume.

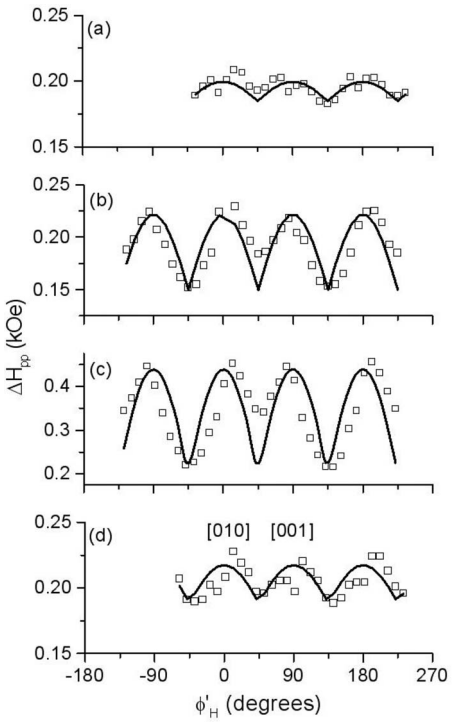

FIG. 9. The in-plane ferromagnetic resonance linewidth, $\Delta H_{p.p.}$, as a function of angle ϕ'_H for Fe_3O_4 films with d, α values of (a) 45 nm, 2°; (b) 45 nm, 5°; (c) 45 nm, 10°; and (d) 30 nm, 2°. The lines show fits to $\Delta H_{p.p.}=\Delta H_0+(dH_R/d\phi_U)\Delta\phi_U$ with parameters given in the text.

Turning now to the value of $H_{4\|}$ $(=2K_{4\|}/M)$, we note that its value of −305 Oe found for all samples, except the $\alpha=5°$ and 10° films, is similar to that of $2K_{4\|}/M=-380$ Oe obtained by van der Heijden *et al.*[22] for Fe_3O_4 films grown on MgO (100) using MBE. The former value is 65% of that of −466 Oe for magnetite single crystals,[32] which is indicative of a high crystalline quality of these films. We note that the values of $2K_1/M$ for magnetite produced by sputtering and pulsed laser deposition differ substantially from those for the bulk single crystals.[23,33]

B. Angular dependence of the linewidth

The striking feature of the results is the development of a strong in-plane angular dependence of the peak-to-peak linewidth, $\Delta H_{p.p.}$, for the 45 nm thick film as the vicinal angle is increased from 2° to 10°. By contrast, the angular dependence of $\Delta H_{p.p.}$ for $\alpha=2°$ remains rather small as the thickness is changed between 30 and 70 nm. We now seek to explain these features. It is usual to express the linewidth as

$$\Delta H_{p.p.} = \Delta H_{hom} + \Delta H_{inhom},$$

where the homogeneous contribution, ΔH_{hom}, arises from the intrinsic damping of the magnetization and ΔH_{inhom} comes

from the magnetic inhomogeneities of the sample; both can have an angular dependence. The homogeneous contribution is given by[26]

$$\Delta H_{\text{hom}} = \frac{2}{\sqrt{3}} \frac{1}{|\partial\omega/\partial H|} \frac{G}{M^2} \left(\frac{\partial^2 F}{\partial \theta^2} + \frac{1}{\sin^2 \theta} \frac{\partial^2 F}{\partial \phi^2} \right), \qquad (9')$$

where G is the Gilbert damping parameter. We are only concerned with the in-plane linewidth and, in this case, Eqs. (1), (4), and (9) give

$$\Delta H_{\text{hom}} = \frac{2}{\sqrt{3}} \frac{G\omega}{\gamma^2 M} \frac{1}{\cos(\phi - \phi_H)}. \qquad (10)$$

Since in our case the magnetic field used is strong enough to align the magnetization along the applied field direction to within a few degrees, the value of $\phi - \phi_H$, and hence the deviation of $\cos(\phi - \phi_H)$ from unity, is very small. Therefore, this contribution is almost constant and so could not be the cause of the angular variation of the linewidth.

Another possibility is that the angular dependence of the linewidth comes from that of the inhomogeneous contribution ΔH_{inhom}. The magnetic inhomogeneities, arising from sample imperfections, such as mosaic structure and defects, can give rise to a distribution in the directions of both the crystal and magnetic anisotropy axes as well as a spread in the magnitudes of the internal fields so that, following Chappert *et al.*,[34] we may write

$$\Delta H_{\text{inhom}} = + \sum_i \frac{\partial H_R}{\partial \phi_i} \Delta \phi_i + \sum_j \frac{\partial H_R}{\partial H_j} \Delta H_j. \qquad (11)$$

We consider only the in-plane variation and so the angular spread $\Delta\phi_i$ includes spreads in the direction of the axes of the cubic and uniaxial anisotropies and ΔH_j includes spreads in $H_{4\|}$, $H_{2\|}$, and M_{eff}. Several of these terms can be ruled out because they give angular dependencies of ΔH that do not fit to the observed dependencies. The linewidth is found to have maxima at $\phi_H = 0, \pi/2, \pi, \ldots$ with minima in between the two adjacent values. However, Eqs. (4) and (11) imply that a spread in the direction of cubic axes and the magnitudes of $H_{4\|}$, $H_{2\|}$, and M_{eff} would give linewidth maxima at $(\pi/8, 3\pi/8, 5\pi/8, \ldots)$, $(0, \pi/4, 2\pi/4, \ldots)$, and $(\pi/4, 3\pi/4, 5\pi/4, \ldots)$, respectively; none of these match the data. However, a spread, $\Delta\phi_U$, in the direction of the axis of the uniaxial term $H_{2\|}$ does give maxima at $\phi_H = 0, \pi/2, \pi, \ldots$ as observed. The in-plane angular dependence of $\Delta H_{\text{p.p.}}$ calculated on this basis is shown in Fig. 9. The parameters used in the fits are ($\Delta\phi_U = 29°$, $\Delta H_0 = 0.19$ kOe), ($\Delta\phi_U = 23°$, $\Delta H_0 = 0.15$ kOe), ($\Delta\phi_U = 23°$, $\Delta H_0 = 0.20$ kOe), and ($\Delta\phi_U = 29°$, $\Delta H_0 = 0.19$ kOe) for the 45 nm films with $\alpha = 2°$, 5°, 10° and 30 nm film with $\alpha = 2°$, respectively; the other parameters are given in Table I. These angular spreads seem unrealistically large but they may be related to the rugged character of the step edges. The increase in the variation of $\Delta H_{\text{p.p.}}$ as α increases, even though $\Delta\phi_U$ remains nearly constant comes from the increase in $H_{2\|}$.

It is clear from Fig. 9 that the spread $\Delta\phi_U$ does not fully account for the observed linewidth variation as the linewidth for $\boldsymbol{H}$ along [011] and hence perpendicular to the step edges is greater than for $\boldsymbol{H}$ along $[0\bar{1}1]$ and parallel to the edges. However, this difference may arise from two magnon scattering as Arias and Mills[35] have predicted that for stepped surfaces this mechanism will give rise to a maximum linewidth when $\boldsymbol{M}$ is perpendicular to the edges and a minimum when it is parallel; as previously indicated the difference in the direction of $\boldsymbol{M}$ and $\boldsymbol{H}$ should be small in the present case.

In brief, the angular variation of $\Delta H_{\text{p.p.}}$ for the films may be largely accounted for by a combination of that arising from a spread $\Delta\phi_U$ together with two magnon scattering by the steps. With magnon scattering, the values of $\Delta\phi_U$ necessary to provide the required amplitude for variation with period $\pi/2$ would be smaller (and more plausible) than those used for the fits in Fig. 9.

V. CONCLUSIONS

Fe_3O_4 films on vicinal MgO(100) with step edges parallel to $[0\bar{1}1]$ have an in-plane uniaxial anisotropy with easy axis perpendicular to the step edge. The strength of this anisotropy varies approximately quadratically with the vicinal angle. As regards its dependence on film thickness, d, it can be represented by the sum of two terms, one of which is independent of d and the other one proportional to $1/d$. The latter is associated with an anisotropy localized at the interface, most likely at the steps, and the first may be associated with APBs preferentially aligned with the step edges. A second, weaker, in-plane uniaxial anisotropy is present in the film on the 10° miscut substrate, which we attribute to an uneven step edge configuration. The FMR linewidth also exhibits an in-plane anisotropy that increases in magnitude as the vicinal angle increases but is almost independent of thickness, in the range 30–70 nm, of films on the 2° miscut substrate.

*Author to whom correspondence should be addressed; mcguigal@tcd-ie

[1] S. Sugahara and M. Tanaka, Appl. Phys. Lett. **80**, 1969 (2002).
[2] B. Degroote, M. Major, J. Meersschaut, J. Dekoster, and G. Langouche, Surf. Sci. **482-485**, 1090 (2001).
[3] D. Zhao, Feng Lui, D. L. Huber, and M. G. Lagally, J. Appl. Phys. **91**, 3150 (2002).
[4] Y. Z. Wu, C. Won, and Z. Q. Qiu, Phys. Rev. B **65**, 184419 (2002).
[5] R. K. Kawakami, Ernesto J. Escorcia-Aparicio, and Z. Q. Qiu, Phys. Rev. Lett. **77**, 2570 (1996).
[6] T. Leeb, M. Brockmann, F. Bensch, S. Miethaner, and G. Bayreuther, J. Appl. Phys. **85**, 4964 (1999).
[7] J. Chen and J. L. Erskine, Phys. Rev. Lett. **68**, 1212 (1992).
[8] H. J. Choi, Z. Q. Qiu, J. Pearson, J. S. Jiang, Dongqi Li, and S. D. Bader, Phys. Rev. B **57**, R12713 (1998).

[9] H. J. Elmers, J. Hauschild, and U. Gradmann, J. Magn. Magn. Mater. **221**, 219 (2000).
[10] V. Usov, S. Murphy, and I. V. Shvets, J. Appl. Phys. **95**, 7312 (2004).
[11] D. M. Engebreston, J. Berezovsky, J. P. Park, L. C. Chen, C. J. Palmstrom, and P. A. Crowell, J. Appl. Phys. **91**, 8040 (2002).
[12] R. K. Kawakami, M. O. Bowen, H. J. Choi, E. J. Escorcia-Aparicio, and Z. Q. Qiu, Phys. Rev. B **58**, R5924 (1998).
[13] A Berger, U. Linke, and H. P. Oepen, Phys. Rev. Lett. **68**, 839 (1992).
[14] B. B. Maranville, A. L. Shapiro, and F. Hellman, Appl. Phys. Lett. **81**, 517 (2002).
[15] F. Walz, J. Phys.: Condens. Matter **14**, R285 (2002).
[16] D. T. Margulies, F. T. Parker, M. L. Rudee, F. E. Spada, J. N. Chapman, P. R. Aitchison, and A. E. Berkowitz, Phys. Rev. Lett. **79**, 5162 (1997).
[17] F. C. Voogt, T. T. M. Palstra, L. Niesen, O. C. Rogojanu, M. A. James, and T. Hibma, Phys. Rev. B **57**, R8107 (1998).
[18] S. Celotto, W. Erenstein, and T. Hibma, Eur. Phys. J. B **36**, 271 (2003).
[19] R. G. S. Sofin, S. K. Arora, and I. V. Shvets, J. Appl. Phys. **97**, 10D315 (2005).
[20] S. K. Arora, R. G. S. Sofin, and I. V. Shvets, Phys. Rev. B **72**, 134404 (2005).
[21] M. Farle, Rep. Prog. Phys. **61**, 755 (1998).
[22] P. A. A. van der Heijden, M. G. van Opstal, C. H. W. Swuste, P. H. J. Bloemen, J. M. Gaines, and W. J. M. de Jonge, J. Magn. Magn. Mater. **182**, 71 (1998).
[23] B. Atkas, Thin Solid Films **307**, 250 (1997).
[24] K Balakrishnan, S. K. Arora, and I. V. Shvets, J. Phys.: Condens. Matter **16**, 5387 (2004).
[25] X. Liu and J. K. Furdyna, J. Phys.: Condens. Matter **18**, R245 (2006).
[26] H. Suhl, Phys. Rev. **97**, 555 (1955).
[27] J. Smit and H. G. Beljers, Philips Res. Rep. **10**, 113 (1955).
[28] R. Naik, C. Kota, J. S. Payson, and G. L. Dunifer, Phys. Rev. B **48**, 1008 (1993).
[29] B. Heinrich, S. T. Purcell, J. R. Dutcher, K. B. Urqhart, J. F. Cochran, and A. S. Arrott, Phys. Rev. B **38**, 12879 (1988).
[30] L. R. Bickford, Jr., Phys. Rev. **78**, 449 (1950).
[31] Par M. Louis Neel, J. Phys. Radium **4**, 15 (1954).
[32] B. A. Calhoun, Phys. Rev. **94**, 1577 (1954).
[33] S. Kale, S. M. Bhagat, S. E. Lofland, T. Scabarozi, S. B. Ogale, A. Orozco, S. R. Shinde, T. Venkatesan, B. Hannoyer, B. Mercey, and W. Prellier, Phys. Rev. B **64**, 205413 (2001).
[34] C. Chappert, K. L. Dang, P. Beauvillain, H. Hurdequint, and D. Renard, Phys. Rev. B **34**, 3192 (1986).
[35] R. Arias and D. L. Mills, Phys. Rev. B **60**, 7395 (1999).